Title
Probing the structural basis and adsorption mechanism of an enzyme on nano-sized protein carriers

Journal
Nanoscale, 9(10)

ISSN
2040-3364

Authors
Pan, Yanxiong
Neupane, Sunanda
Farmakes, Jasmin
et al.

Publication Date
2017-03-09

DOI
10.1039/c7nr00276a

Nanoscale

PAPER

View Article Online
View Journal | View Issue

Cite this: *Nanoscale*, 2017, **9**, 3512

Probing the structural basis and adsorption mechanism of an enzyme on nano-sized protein carriers†

Yanxiong Pan,‡[a] Sunanda Neupane,‡[a] Jasmin Farmakes,[a] Michael Bridges,[b] James Froberg,[c] Jiajia Rao,[d] Steven Y. Qian,[e] Guodong Liu,[a] Yongki Choi[c] and Zhongyu Yang*[a]

Silica nanoparticles (SiNPs) are important nano-sized, solid-state carriers/hosts to load, store, and deliver biological or pharmaceutical cargoes. They are also good potential solid supports to immobilize proteins for fundamental protein structure and dynamics studies. However, precaution is necessary when using SiNPs in these areas because adsorption might alter the activity of the cargoes, especially when enzymes are loaded. Therefore, it becomes important to understand the structural basis of the cargo enzyme activity changes, if there is any. The high complexity and dynamics of the nano–bio interface present many challenges. Reported here is a comprehensive study of the structure, dynamics, and activity of a model enzyme, T4 lysozyme, upon adsorption to a few surface-modified SiNPs using several experimental techniques. Not surprisingly, a significant activity loss on each studied SiNP was found. The structural basis of the activity loss was identified based on results from a unique technique, the Electron Paramagnetic Resonance (EPR) spectroscopy, which probes structural information regardless of the complexity. Several docking models of the enzyme on SiNPs with different surfaces, at different enzyme-to-SiNP ratios are proposed. Interestingly, we found that the adsorbed enzyme can be desorbed *via* pH adjustment, which highlighted the potential to use SiNPs for enzyme/protein delivery or storage due to the high capacity. In order to use SiNPs as enzyme hosts, minimizing the enzymatic activity loss upon adsorption is needed. Lastly, the work outlined here demonstrate the use of EPR in probing structural information on the complex (inorganic)nano–bio interface.

Received 12th January 2017,
Accepted 16th February 2017

DOI: 10.1039/c7nr00276a

rsc.li/nanoscale

Introduction

Nanotechnology has advanced many areas of life over the past few decades. The involved nanomaterials, especially nanoparticles (NPs), often have unique chemical, electrical, optical, and magnetic properties, depending on the chemical composition, such as metals, inorganics, organic molecules, or block polymers, as well as their particle sizes and surface functional groups. An attractive area for the use of NPs, especially the nonporous silica nanoparticles (SiNPs), is to house enzymes for enhancing catalysis efficiency[1–3] and to carry and deliver genes and even prodrug molecules.[4–6] Of particular interest to us is to immobilize enzymes onto the nonporous SiNPs. Immobilization of enzymes helps increase the environmental tolerance of enzymes, prevents enzyme aggregation and/or unfolding, and allows for the reuse of the host.[2] Compared to other NP hosts/carriers, the SiNPs have straightforward preparation, relatively low-cost, and good biocompatibility.[7] While most enzyme immobilization were realized *via* covalent bonding of the enzyme to the nonporous SiNPs, it is also promising to attach enzymes *via* non-covalent interactions (*ca.* charge–charge interaction). In doing so, the potential enzyme structural restriction caused by covalently linking one site of the enzyme to the solid phase can be minimized. It also makes it possible to detach the enzyme from the solid host.

[a]*Department of Chemistry and Biochemistry, North Dakota State University, Fargo, ND, 58108, USA. E-mail: zhongyu.yang@ndsu.edu*
[b]*Jules Stein Eye Institute, University of California, Los Angeles, CA, 90025, USA*
[c]*Department of Physics, North Dakota State University, Fargo, ND, 58108, USA*
[d]*Department of Plant Sciences, North Dakota State University, Fargo, ND, 58108, USA*
[e]*Department of Pharmaceutical Sciences, North Dakota State University, Fargo, ND, 58108, USA*

†Electronic supplementary information (ESI) available: Procedures for protein expression, purification, and spin labeling; preparation of silica nanoparticles; characterization of silica nanoparticles; details of EPR and activity assays; instrumentation descriptions and supporting data of FTIR, zeta potential, and CW and DEER EPR spectroscopy. See DOI: 10.1039/c7nr00276a

‡These authors contributed equally.

Another potential application of SiNPs is to serve as hosts to immobilize proteins to probe protein structure and dynamics information at the molecular level. This area has important potential to be explored because the complications caused by the protein rotational tumbling can be effectively removed.[8,9] For example, the continuous wave (CW) electron paramagnetic resonance (EPR) in combination with Site-Directed Spin Labelling (SDSL)[9] probes protein backbone dynamics in a site-specific manner. This approach relies on the close relationship between the EPR line shape and the spin label motion, which includes both protein rotational tumbling and backbone dynamics. For smaller proteins (<45 kDa), the rotational tumbling dominates the line shape and washes off its sensitivity to backbone motion. An effective approach to avoid protein rotational tumbling is to immobilize the target protein onto a solid support. A common approach to immobilize proteins is *via* the CNBr-activated sepharose beads.[10,11] The surface charges of SiNPs are often tunable, making it possible to immobilize proteins *via* non-covalent bonding and the adsorption reversible. Taken together, SiNPs as hosts and/or carriers are important in both nanotechnology and protein science.

One of the major concerns in utilizing these SiNPs to carry or host enzymes is the possible enzymatic activity loss caused by the molecular interaction between the SiNPs and the cargo enzymes. A common consequence when an enzyme is adsorbed to a carrier is the structural and/or conformational changes upon adsorption, the scale of which are often associated with the activity loss at various levels.[12–15] In addition, the surrounding biomolecules may also reduce the enzymatic activity of the cargo enzyme, by either blocking the access of substrates or replacing the adsorbed enzyme molecules.[16,17] Therefore, understanding the structure–function relationship of cargo enzyme on SiNP surface in the biological environment becomes an essential task in nanobiotechnology.

When adsorbed to the SiNP surface, the enzyme molecules usually form two layers of the well-known protein corona: the hard corona and the soft corona.[17–23] While the soft corona contains protein loosely adsorbed, the hard corona is formed by proteins tightly adsorbed to the SiNP, which is, therefore, the corona layer where the enzymes function and the focus of most studies on enzyme-carrier complexes. While exciting progress has been made to help understand the hard corona, the structural basis of the enzymatic activity loss and the relative orientations of the enzymes upon adsorption to their SiNP carriers still need to be elucidated. Full understanding of these interactions are challenging to obtain, mainly due to the large size of and the difficulty to co-crystallize the protein/SiNP complexes as well as the high heterogeneity and dynamics of the protein–SiNP interaction ("dynamic corona").

Reported here is a comprehensive study to probe the structure, dynamics, and function of a model enzyme, T4 lysozyme (T4L), upon adsorption to a few surface-modified SiNPs using the EPR spectroscopy in combination with several other analytical techniques. Prior to this work EPR has been mainly applied to probe structure information in complex biological or synthetic systems.[24–37] The technical advantage of EPR in these studies is the capability to probe structure and dynamics information of macromolecules in their native states, regardless of the size and complexity.[38] Particular information EPR provides are long-range (a few nm) intra-macromolecular distance distributions[39,40] and site-specific conformational dynamics in a broad time window (ns to ms).[9,41] Comparing to other experimental techniques, EPR has some unique advantages which make it a good complimentary approach. For example, the size limitation of NMR-based structural determination can be removed by EPR. In comparison to the large fluoro-labels, the small EPR spin label causes minimal structural perturbation to the target macromolecules and results in smaller uncertainties in distance measurements.[38] EPR is able to probe macromolecules in their native states, which is particularly helpful for systems that are difficult to crystallize. Based on two EPR techniques, the CW[9] and the Double Electron–Electron Resonance (DEER)[40] EPR, the dynamic and structural changes of T4L enzyme upon adsorption to these surface-modified SiNPs were characterized. The average number of adsorbed proteins per SiNP was estimated and the residues that are responsible for making contact with each SiNP surface and other enzymes (when the SiNPs were fully loaded) were identified *via* CW EPR. Then, the extent of structural changes was probed *via* DEER. Interestingly, it was found that the adsorbed enzyme can be released *via* pH adjustment, highlighting the possibility of using two of the studied SiNPs to perform controlled release of cargo enzymes. Lastly, possible structural models for enzyme adsorption to different SiNPs are proposed.

Results and discussion

T4L is a good model enzyme for our study for several reasons. It cleaves glycosidic linkages in the peptidoglycan of bacterial cell walls.[42] The intrinsic flexibility of T4L is closely correlated to its enzymatic activity, which serves as a good model to investigate the structure–function relationship of enzymes.[43,44] In addition, T4L has been investigated with EPR in solution and other medium with data well-interpreted in literature, making it a good reference protein for EPR study.[45] Due to its relatively small size (18.7 kDa), the CW EPR spectrum of spin-labeled T4L is dependent on the intrinsic motion of the spin label, the local backbone dynamics of the labeled site, and the rotational tumbling of the protein molecule.[9,10,38] Upon adsorption onto the SiNPs, the rotational tumbling of the enzyme molecules is severely restricted, causing a significant change (broadening) in CW EPR line shape. This change can be used to indicate and monitor the behavior of the protein in the protein–SiNP complex.[8] Lastly, T4L has a positive net charge at the pH 7, making it possible be adsorbed by SiNPs.

To employ EPR, the SDSL is often employed to implant a paramagnetic spin label to the desired site of the target protein.[27,46] In SDSL, a cysteine residue is generated *via* site-directed mutagenesis, followed by reaction with a methane-

thiosulfonate spin labeling (MTSL) reagent to form a disulfide bond with the cysteine.[8,47] The so-generated protein side chain is often named as "R1".[47] It has been demonstrated that attaching an R1 sidechain at a number of sites in T4L does not alter the function or the secondary structure of the protein.[8,9,48,49] In order to evaluate the effects of surface charge and functional groups on enzyme adsorption, three SiNPs were prepared, the amine-, the hydroxyl- and the carboxyl-coated SiNPs, the net charge of which is positive, negative, and negative at pH 7, respectively (from now on we designate them as NH2-SiNPs, OH-SiNPs, and COOH-SiNPs, respectively, for simplicity).

Characterization of the model protein and SiNPs

A total of eight T4L mutants were spin labeled for our study (the spin-labeled mutants were named as *x*R1 where *x* is the residue being mutated). These mutants essentially scan through the whole protein. The enzyme mutants expressed and spin-labeled in our laboratory were confirmed to have native secondary structure and activity using the Circular Dichroism (CD) spectroscopy and an activity assay,[43] respectively. In addition, the CW-EPR spectra of the spin-labeled mutants were acquired to confirm the local conformational dynamics of the labeled sites to be identical to those reported in the literature (Fig. S1†).[8,48,49] The involved SiNPs were prepared as described in the ESI† and characterized using the Fourier Transformation Infrared (FTIR) spectroscopy (Fig. S2A†), the zeta potential measurements (Fig. S2B†), and the Transmission Electron Microscopy (TEM). As shown in Fig. 1, the TEM indicated that the average diameters of the OH-SiNPs and the COOH-SiNPs were ~30 nm. The NH2-SiNPs, however, were severely aggregated. Therefore, no TEM image was attempted for the NH2-SiNPs. The surface charge of each SiNP was as expected as determined by the zeta potential measurements (*cf.* Fig. S2B and ESI† text).

TEM images depict the adsorption of T4L onto SiNPs

One of the best ways to depict and confirm enzyme adsorption to SiNPs is to visualize the change in TEM upon enzyme adsorption. Therefore, the TEM images of T4L adsorbed to the OH- and the COOH-SiNPs (enzyme-to-SiNP ratio ~10 000 : 1) after incubation for ~30 min were acquired. The resultant mixtures were washed extensively to remove non-adsorbed enzymes (the SiNPs were "fully saturated" with T4L). The phosphotungstic acid was used to stain molecules outside of the nanoparticles. As shown in Fig. 1C and D, the dark areas surrounding each particle clearly indicate the adsorption of T4L onto SiNPs.

Atomic force microscopy (AFM) images confirm the enzyme adsorption

AFM imaging provides direct visualization of enzyme adsorption with higher resolution. The AFM images of the COOH- and the OH-SiNPs in the absence and presence of T4L adsorption (enzyme-to-SiNP ratio ~10 000 : 1) were acquired. As shown in Fig. 2A (images 1, 2, 5, & 6), without enzyme the images of the two SiNPs are indistinguishable. Upon enzyme

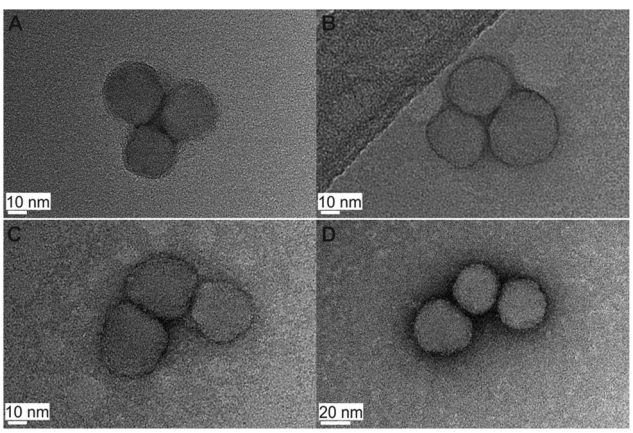

Fig. 1 TEM images of the OH-SiNPs (A) and the COOH-SiNPs (B) in water. The approximate particles diameter is 30 nm in each case. Upon saturation of the OH-SiNPs (C) and the COOH-SiNPs (D) with the T4L 44R1 mutant, a clear black layer coating each SiNP is evident, indicating the adsorption of enzyme on SiNPs. Abbreviations are defined in the main text.

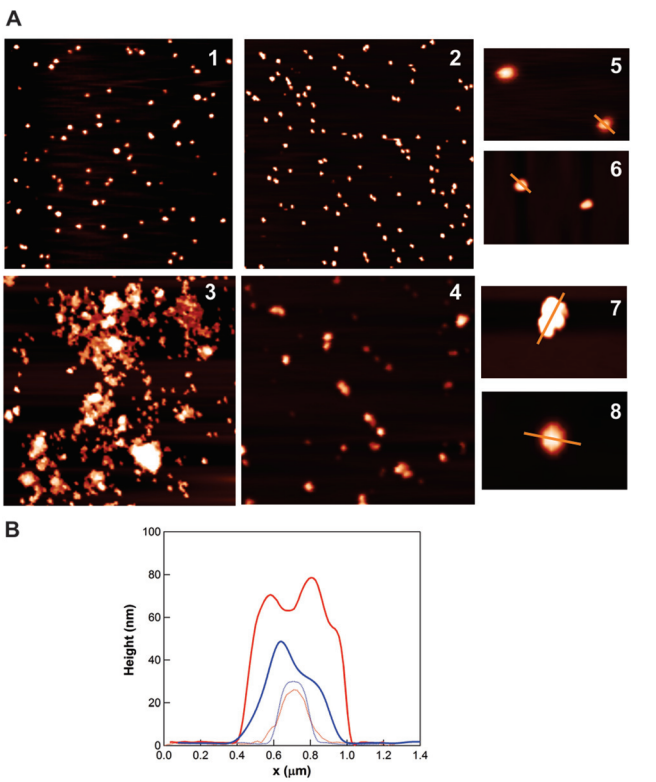

Fig. 2 (A) AFM images for 1: COOH-SiNP, 2: OH-SiNP, 3: T4L-COOH-SiNP, 4: T4L-OH-SiNP (10 μm × 10 μm). The *z* scale is 0–30 nm for images 1 and 2 and 0–120 nm for images 3 and 4. Images 5, 6, 7, 8 are the zoom of images 1, 2, 3, 4, respectively (2 μm × 1.3 μm). The *z* scale is 0–30 nm for images 1, 2, 5, and 6 and 0–120 nm for images 3, 4, 7, and 8. (B) The height image: blue-dotted = 5, red-dotted = 6, blue = 7, and red = 8.

adsorption, the particle sizes are clearly increased (Fig. 2A). Furthermore, the overall size of the COOH-SiNPs (Fig. 2A, images 3 & 7) is larger than that of the OH-SiNPs (Fig. 2A, images 4 & 8), indicating more enzymes were adsorbed to the COOH-SiNPs. The height image (Fig. 2B) shows a better view, wherein protein adsorption increases the size of the particle, and there is apparently more proteins adsorbed to the COOH-SiNPs (Fig. 2B, red *vs.* blue).

Probing the loading capacity of the hard corona

A key character of the SiNP-based enzyme carriers is the loading capacity. To probe this, we prepared a series of mixtures with increasing T4L-to-SiNP ratio for the OH- and the COOH-SiNPs. After an incubation of at least 30 min, the supernatant of each sample was separated from the mixture *via* centrifugation (2000 rpm, 5 min). The amount of adsorbed protein at each ratio can be computed by subtracting the amount of protein in the supernatant from the total added protein. The adsorption profile was then obtained by plotting the amount of adsorbed protein as a function of the added T4L-to-SiNP ratio. There was essentially no adsorption on the NH2-SiNPs, as most added proteins remained in the supernatant. This is expected since, at pH 7.0, T4L and NH2-SiNPs repulse each other due to their positive surface charges. Both the OH- and the COOH-SiNPs showed a clear indication of T4L adsorption. The adsorption profile of the OH-SiNPs, as shown in Fig. S3,† indicates that as the T4L-to-SiNP ratio is increased, the amount of bound protein is increased. A plateau is reached with ~3500–4000 protein per SiNP. Such adsorption is most likely due to the opposite surface charges of T4L and the OH-SiNPs. Interestingly, the COOH-SiNPs were so well-separated and dispersed that, our attempts to separate the supernatant from the mixture failed. The small amount of remaining COOH-SiNPs in the supernatant contributed to the UV absorption and complicated our measurements. We therefore did not obtain any reproducible, convincing adsorption profile for the COOH-SiNPs. A technique which is not so sensitive to the dispersed COOH-SiNPs should be used.

EPR area analysis to estimate the SiNP-carrier loading capacity

The principle of using EPR area analysis to probe the amount of adsorbed proteins is based on the fact that the amount of (spin-labeled) protein is proportional to the CW EPR spectral area. The CW EPR spectra of a mutant before and after washing with water can be compared. The percentage of the adsorbed proteins can be estimated by computing the loss in the spectral area due to washing. It is worth noting that the EPR samples were washed *via* the same procedure as in the previous section. However, the small amount of suspended COOH-SiNPs in the supernatant did not present to be a major problem because the majority of the COOH-SiNPs were settled to the pellet; the uncertainty in loading capacity estimation caused by these suspended particles is negligible. This EPR approach is less sensitive to the presence of SiNPs, therefore providing a close estimation of the enzyme loading capacity. In addition, as mentioned above, the restriction of enzyme rotational tumbling due to adsorption on SiNPs results in a broadened EPR spectrum, while the unbound enzymes often show a relative sharper spectrum.

The mutant we selected for such study was 44R1 since the "broad" spectral component of its spectrum is well-separated from its sharp component (see data below). We started with 10 000 : 1 and 15 000 : 1 protein-to-NP ratio for the OH- and COOH-SiNPs, respectively. After mixing and incubation, ~20 μL sample was loaded to the EPR capillary. This volume is the effective volume of our cavity resonator. It is important to use this sample volume so that both the adsorbed and the unbound proteins are being detected. Loading a sample with a larger volume will result in missing the detection of the unbound enzyme since the SiNPs tend to settle down to the bottom of the capillary. As shown in Fig. 3, both the 44R1/OH-SiNP and the 44R1/COOH-SiNP sample showed a broad and a sharp peak in the low field region before wash (black curves). Upon washing, the unbound or loosely bound proteins were removed as judged by the disappearance of the sharp peak in Fig. 3. For the COOH-SiNPs, washing only removed the sharp component; both the intensity and the line shape of the broad component are almost unaffected (Fig. 3A). This indicates that most likely washing did not remove the enzymes already adsorbed. The area loss due to wash is ~43%, corresponding to ~6400 protein molecules adsorbed onto each COOH-SiNP. For the OH-SiNPs, the first round of wash not only removed the sharp spectral component but also reduced the intensity of the broad component by ~50% (*cf.* black rectangle of Fig. 3B).

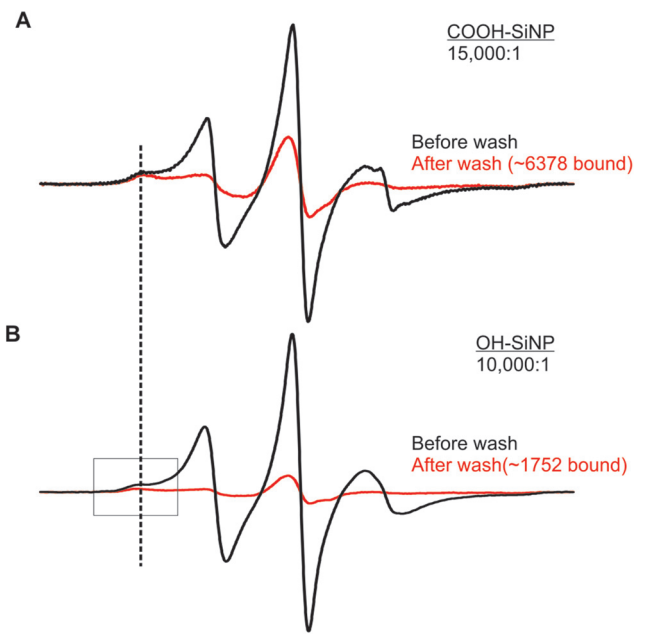

Fig. 3 The CW EPR spectra of the 44R1 adsorbed to the COOH-SiNPs (A) and the OH-SiNPs (B) with a protein-to-SiNP ratio of 15 000 : 1 and 10 000 : 1, respectively, before (black) and after wash (red) with water. The gray rectangle is to highlight the loss of the peak intensity. The dotted line is to illustrate the peak position shift between the spectra on different SiNPs.

This indicated that the adsorption of the enzyme to the OH-SiNPs was most likely labile and could be easily disturbed. Further wash, however, did not decrease the intensity of the broad component. The area analysis indicated that ~1750 proteins were adsorbed onto each OH-SiNP. Note that this number is less than that estimated by the adsorption profile (Fig. S3†). The discrepancy is caused by the fact that there was no wash in the adsorption profile studies (Fig. S3†). In fact, given the 50% loss in the intensity of the broad peak, we anticipated ~3500 proteins per OH-SiNP if no wash was carried out in the EPR study, which is close to that estimated by the adsorption profile (Fig. S3†). Given the relatively small diameter of SiNPs (~30 nm), the large number of bound enzyme indicates a multiplex adsorption scheme (see later discussions). The enzyme washed off during the EPR experiments was found to be functionally active (data not shown). There was essentially no EPR signal from the NH2-SiNPs after washing, consistent with the fact that all proteins remained in the supernatant upon mixing with the NH2-SiNPs.

In principle, the relative population of the adsorbed protein can be estimated with EPR spectral analysis.[9] However, we were not successful in such an attempt because the adsorbed protein might very likely be in a heterogeneous conformation, and it is difficult to account for the broadened spectral component with theoretical models/simulations. Note that the line width of the 44R1 on OH-SiNPs is slightly broader than on the COOH-SiNPs (*cf.* dotted vertical line). This indicates that the enzymes on the OH-SiNPs might have higher conformational heterogeneity than those on the COOH-SiNPs (more discussions see below).

Caution is needed when measuring the adsorption capacity, given the low dispersity of the OH-SiNPs. In fact, partial aggregation of the SiNPs might lead to uncertainties in the estimated loading capacity. Specifically, the gaps between particles may trap enzyme molecules, yielding a larger capacity. Meanwhile, the aggregation may decrease the surface area, leading to a lower capacity. Therefore, before loading enzyme, we sonicated the SiNPs to ensure dispersion. After adsorption, prior to EPR measurements, the samples were always mechanically vibrated. Even so, our dynamic light scattering (DLS) measurements still indicated a polydispersity in the hydrodynamic radii of SiNPs (see ESI†). Therefore, the adsorption capacity reported here is only the average number of adsorbed protein per SiNP.

Enzymatic activity loss upon adsorption to SiNPs

To probe the enzymatic activity of T4L upon adsorption, we selected the 44R1 to be consistent with the previous adsorption capacity studies. Only the OH- and the COOH-SiNPs were involved since the NH2-SiNPs showed no adsorption. The T4L-to-SiNP ratios were selected with some extra caution. Due to the high loading capacity of enzymes on both SiNPs (see above), it is very likely the enzymes pack to form multiple layers of enzymes on the SiNP surface (calculations see below). The enzymes in the inner layer(s) are likely to lose activity due to the shielding of substrates caused by the outer layer enzymes. In addition, even if only a single layer of enzymes is coated on SiNP surface, the contact of T4L with the surface might induce conformational changes of the enzyme, possibly causing activity loss. Therefore it was decided to investigate these two extreme conditions for both the OH- and the COOH-SiNPs. Given the average diameter of ~30 nm, the surface area of a SiNP was estimated to be ~2800 nm^2. Considering the average area that a T4L molecule could occupy (~10–12 nm^2), ~250 proteins adsorbed to the SiNP should form a single layer of protein. Therefore we selected 250 : 1 as the protein-to-SiNP ratio for all our single layer studies. Another case was the multiple layer studies wherein the SiNPs were saturated with T4L. The positive control was to determine the activity of 44R1 in water with no SiNPs. Our negative control experiments were to measure the interaction of the substrates with solely SiNPs.

First it was confirmed that the presence of either SiNPs did not affect the optical density (OD) at 450 nm as shown by our negative controls (see Methods and materials, ESI, and Fig. S4†). To quantitatively evaluate T4L activity upon adsorption to SiNPs, we followed the procedure reported by Bower *et al.*, wherein the activity was characterized by the slope of the initial decay of OD at 450 nm (Fig. 4).[43] In our case, we performed a linear fit to the beginning 40 s of each data set (and converted the slope unit to mA min^{-1} as indicated by ref. 43). When the T4L-to-SiNP ratio was 250 : 1 and the final protein concentration was adjusted to be the same as in the positive control experiments (Fig. 4A and B black curves) for the COOH-SiNPs, the slope of the decrease of OD at 450 nm (green; 90 ± 6 mA min^{-1}; the value after the "±" represents the standard deviation from the fitting) is significantly slower than that of protein in water (black; 204 ± 66 mA min^{-1}), indicating when the enzyme formed a single layer on COOH-SiNPs, there was a significant activity loss. This indicated the single-layer adsorption very likely caused a structural change in T4L. On the OH-SiNPs with the same ratio, the activity loss (blue triangles of Fig. 4B) was even higher, possibly indicating an even larger extent of structural changes. When both SiNPs were saturated with T4L, the concentration of the SiNPs was adjusted to be the same as that in the case of 250 : 1, meaning the adsorbed, final protein concentration was ~6 and ~17 times higher on the OH- and the COOH-SiNPs,

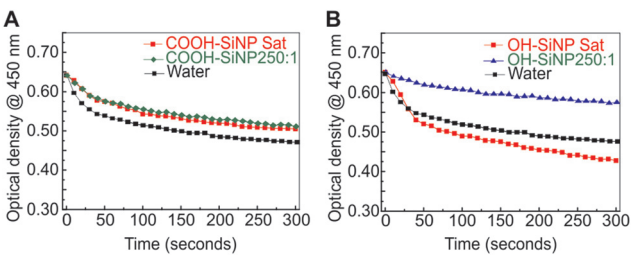

Fig. 4 The activity assay of the 44R1 adsorbed to the COOH-SiNPs (A) and the OH-SiNPs (B) with a protein-to-SiNP ratio of 250 : 1 (green) and when the SiNPs were saturated (red) with the enzyme. The black curve indicates the activity of 44R1 in water without any SiNPs and is reproduced in both figures for comparison.

respectively. Interestingly, for both SiNPs, we did not observe a decrease in OD at 450 nm (102 ± 6 mA min^{-1} for COOH-SiNPs and 186 ± 6 mA min^{-1} for OH-SiNPs) that was consistent with the protein concentration increase. This indicated that when multiple layers of enzymes were formed on SiNPs, the enzymes in the inner layer(s) were inactive, most likely due to the conformational change caused by adsorption/crowding and/or the limited access to the substrates. However, it is unclear why for the enzyme saturated COOH-SiNPs (Fig. 4A, red), the enhancement in activity was only slightly higher than in the case of the single layer protein (and the activity is less than the positive control). A higher mixture viscosity when T4L saturated the COOH-SiNPs was observed, which severely limited the access of substrates. Nevertheless, it is clear that adsorption to SiNPs caused a loss in T4L enzymatic activity.

Probing the origins of the activity loss: site-specific conformational dynamics of the adsorbed enzyme

Due to the close relationship of structure, dynamics, and activity of enzymes, it is speculated that the loss in activity was related to structural and conformational changes. To probe the conformational dynamics of T4L on SiNPs, the EPR spin label was introduced onto eight sites of T4L (including 44R1; *cf.* Fig. 5A). The CW EPR spectra of these eight mutants upon adsorption to SiNPs were found to be broadened in comparison to the same mutants in solution (Fig. 5B–I *vs.* Fig. S1†), for both the single-layer enzyme coated and saturated SiNPs. Since the CW EPR line shape is known to be sensitive to motion of the spin label, probing the origins of such broadening on each site might lead to important structural information of enzyme adsorption.

When an enzyme is adsorbed onto the SiNP surface, three factors are anticipated to cause CW EPR line broadening: (1) contact of the enzyme with the SiNP surface, (2) crowding caused by nearby adsorbed enzymes when multiple layers are formed, and (3) restriction of protein rotational tumbling caused by adsorption and/or crowding. To evaluate the contribution of each factor, a series of control experiments were included wherein T4L mutants were immobilized onto the CNBr-activated sepharose beads. Such attachment completely restricted the protein rotational tumbling due to the formation of covalent bonds between the –CN groups on the sepharose surface and the protein amines (lysines). In this case, if there were any line broadening, it must be contributed by the factor 3 (see above). Contributions from factors 1 and/or 2 were removed.

When a single enzyme layer was formed on SiNPs, by comparing the spectra of T4L mutants on SiNPs with those of the same sites on the sepharose, sites were identified that show additional broadening. These sites must be those making contact with the SiNP surface since factor 3 did not exist in this case. As shown in Fig. 5(B–I), a comparison of the black and the dotted curves in the low field region (rectangle) of each mutant yields that almost every studied site shows an additional peak (*e.g.* arrows in Fig. 5C and H), with 151R1 exhibiting the least low-field peak intensity (as comparing to

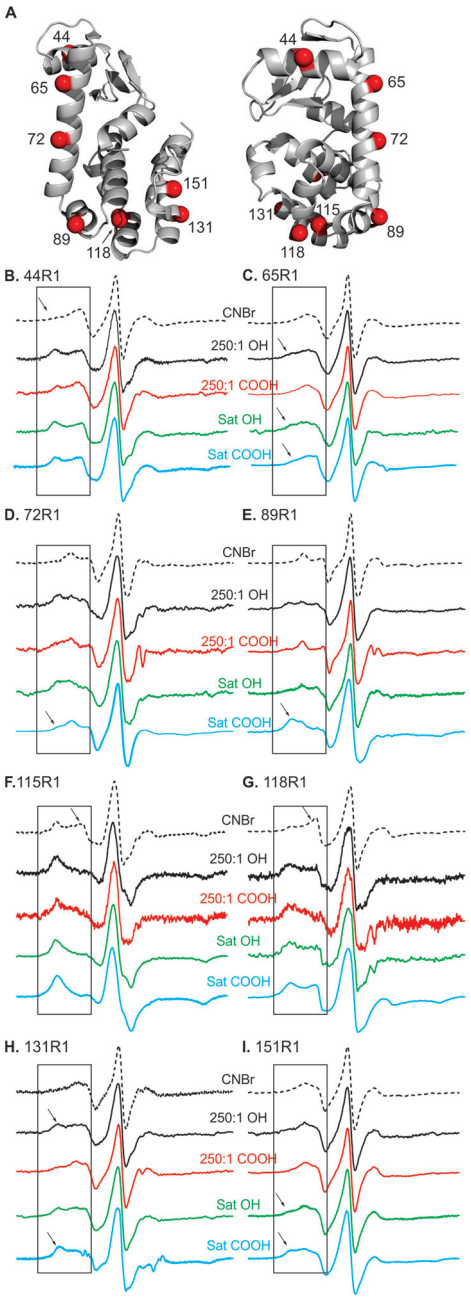

Fig. 5 (A) The crystal structure of the T4L (pdb: 3lzm) and the Cα of the residues that were mutated and spin labeled (red spheres) viewed at two angles. (B)–(I) The CW EPR spectra of each spin labeled mutant when attached to the CNBr-activated sepharose beads (dotted black) and when adsorbed to the OH-SiNPs (black and green) and the COOH-SiNPs (red and blue). The black and red curves indicate the spectra taken from samples when the T4L-to-SiNP ratio was 250 : 1, while the green and blue curves indicate the spectra of 44R1 when the corresponding SiNPs were saturated. The rectangle in each figure is to highlight the spectral region where the spectral line shape changes are the most evident between different solid supports. The arrows are to help guide the identification of the spectral changes. Specifically, the arrow in (B) indicates that the pointed low field peak was populated on other solids; arrows in (F), and (G) indicate the reduction in peak intensity; arrows in other figures indicate an increase in peak intensity.

arrows in Fig. 5I). This indicates that when forming a single layer on the OH-SiNPs, T4L are adsorbed to the SiNP in a random orientation wherein any residues with positive surface charges could be contacting the SiNPs. In contrast, on the COOH-SiNPs (red curves in Fig. 5B–I), there is almost no additional peak shown in the spectra of 65R1 and 151R1 (solid red *vs.* dotted black). The broadening in 72R1, 89R1, and 131R1 are also much less in extent as compared to the cases when the same mutants are adsorbed to the OH-SiNPs. The spectra of 44R1, 115R1, and 118R1 show strong broadening, which indicates that likely on the COOH-SiNPs T4L has a preference to contact SiNP surface *via* regions close to residues 44 and 115/118 and *via* regions close to residues 72, 89, and 131 with a lower preference.

When both SiNPs were saturated with T4L, the CW EPR spectra of spin-labeled mutants were compared with those when a single protein layer was formed on the same SiNPs. Sites showing additional broadening indicate regions of T4L that are facing more restriction in motion, most likely due to crowding. For the OH-SiNPs, we found almost no additional broadening (green *vs.* black curves in Fig. 5) for all studied sites, meaning the crowding effects on the OH-SiNPs were not significant. This means the interaction between multiple protein layers is not strong enough to cause additional restriction to the motion the spin labeled sites. This is a reasonable finding because proteins in the first layer are randomly orientated so adsorption of proteins to the next layers is also expected to be non-specific. Such non-specific adsorption is often not enough to create strong inter-enzyme interactions (to generate additional crowding effects). For the COOH-SiNPs, when comparing the red and the green curves (Fig. 5B–I), additional broadening is observed on sites 44R1, 65R1, 89R1, 131R1, and 151R1, indicating that these sites are affected by strong crowding effects when multiple layers of proteins are formed. This finding indicates that, since proteins in the first layer are adsorbed with certain preferred orientations, the adsorption of proteins to the next layers is also likely to have a preference in terms of contact sites and orientation. These specific intermolecular interactions are possibly strong enough to create additional packing/crowding between proteins in the multiple enzyme layers. The stronger inter-enzyme interaction also helps increase the loading capacity of the enzyme on the COOH-SiNPs (see above discussions of Fig. 3).

Probing the origins of the activity loss: intra-protein structural changes upon adsorption to SiNPs

In addition to the local conformational dynamics of T4L upon adsorption, the intra-protein structural changes were also probed with another EPR technique, DEER. DEER EPR spectroscopy is a pulsed EPR technique which relies on probing the magnetic dipolar interaction between two electron spin centers and extracting the distance distribution probability between the two centers.[50] A great advantage of such pulsed dipolar spectroscopy[39,51] is that the distance distribution profile not only reflects the average intra-protein distance but also the conformational ensemble of the studied protein. In our case, the more conformations the protein spans, the broader the distance distribution is detected. To conduct DEER measurement, we created two cysteine mutations on one protein and spin labeled both. A total of three cysteine pairs (Fig. 6A) were selected to probe the effects of adsorption to SiNPs on the global structure of T4L. For all DEER samples, both SiNPs were saturated by T4L. As shown in Fig. 6B–D, for each spin pair, the distance distribution of protein on SiNPs (Fig. 6, black and red curves; data analysis see Fig. S5 and ESI†) is much broader than that of the same pair in buffer (see grey shades of Fig. 6).[52] This indicates a significant amount of extra protein conformations are induced by adsorption. This is not surprising since the crowding is very likely to change the protein conformation when SiNPs are saturated with T4L. A more careful look at the differences between the black and the red curves leads to the trend that proteins on OH-SiNPs have slightly broader distribution, and therefore slightly more conformations than proteins on the COOH-SiNPs. This is consistent with the CW EPR results wherein the low field peak of 44R1 on the OH-SiNPs is broader than that of 44R1 on the COOH-SiNPs (Fig. 3, dotted line). The structural perturbation caused by adsorption to the SiNPs was also observed from the CD measurement, wherein the secondary structure of the enzyme upon adsorption to the SiNPs was found to be perturbed as well (details see ESI†).

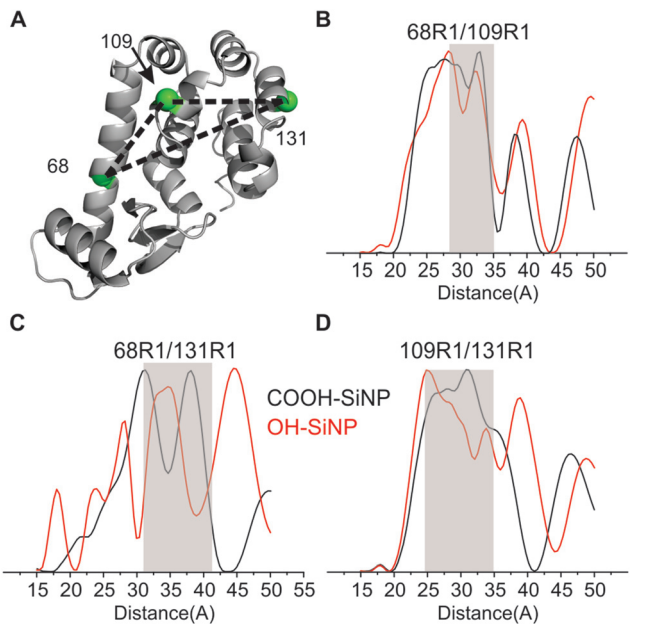

Fig. 6 (A) The crystal structure of the T4L (pdb: 3lzm) and the Cα of the three residue pairs that were mutated and spin labeled (green spheres). Dotted lines indicate the intra-protein distances measured in each DEER experiment. (B)–(D) The distance distribution of each spin-labeled cysteine pair when adsorbed to the COOH-SiNPs (black) and the OH-SiNPs (red). DEER data analysis is provided in the main text and the ESI.† The gray areas indicate the distance distribution of the corresponding pair when protein is in the spin buffer. There is a clear broadening upon adsorption to the SiNPs, indicating an increase in protein conformational states.

Differences in the structural basis of enzyme adsorption between the two SiNPs

The discussion above indicates T4L has a broader range of protein conformation caused by contacting with the OH-SiNP surface and/or crowding, while on the COOH-SiNPs T4L has relatively more uniform conformation. Such finding can be rationalized to the fact that, in addition to the electrostatic interaction between COOH-SiNP and T4L, the additional C═O bonds may serve as proton acceptors to help establish and stabilize hydrogen bonding, which helps stabilize the protein and regulate the protein conformation alignment on the surface of the COOH-SiNPs. The longer linker between the COOH and SiNP surface (see "Methods and materials" and ESI† for SiNP preparation) also possibly provides additional flexibilities to regulate protein conformation.

Desorption of enzyme: reversible adsorption

Since the adsorption of T4L enzyme on these SiNPs was due to the charge–charge interaction, it must be possible to desorb the enzyme from the SiNPs *via* adjusting the SiNP surface charge. Based on the zeta potential measurements at various pH (see Fig. S2B†), the wash solution was selected to have a pH of 3.0 in 0.01 M NaCl. Under this condition, the surface charge of the OH- and the COOH-SiNPs was ~zero and slightly positive, respectively, which should cause desorption of enzyme. Indeed, for both SiNPs, we found almost all adsorbed proteins were detached, as judged by the complete loss in CW EPR intensity and the enzymatic activity when the SiNPs were studied after wash. The eluted enzymes after switching to water medium were found to have identical CW EPR spectra as the same mutants in water (Fig. S7†). The eluted enzymes were also found to be functionally active as judged by the activity assay. The recovery rate was close to 100% after two rounds of wash. Lastly, the washed SiNPs were able to be "reloaded" with fresh T4L; the conformation and activity of the reloaded protein were found to be identical as those discussed before, indicating the SiNPs can be reused.

Possible docking models

At pH 7.0, the surface charge of T4L was estimated *via* the APBS function of PyMOL and shown in Fig. 7. As expected, positive surface charges dominate the protein (see blue *vs.* red). For the OH-SiNPs, although the spin labeled sites (Fig. 7) are close to either negatively or positively charged areas, the local charges of the protein most likely did not form strong electrostatic interactions with the surface of the OH-SiNP, since no specific sites were found to make contact with the SiNP (Fig. 5 and discussion above). This might due to the relatively less negative surface charge and relatively short linker length (comparing to the COOH-SiNPs) between the –OH groups and the Si on the surface, the latter of which may present some hindrance for protein adsorption. It is also possible that other molecular interactions (*e.g.* the van der Waals force) contribute to the adsorption. Nevertheless,

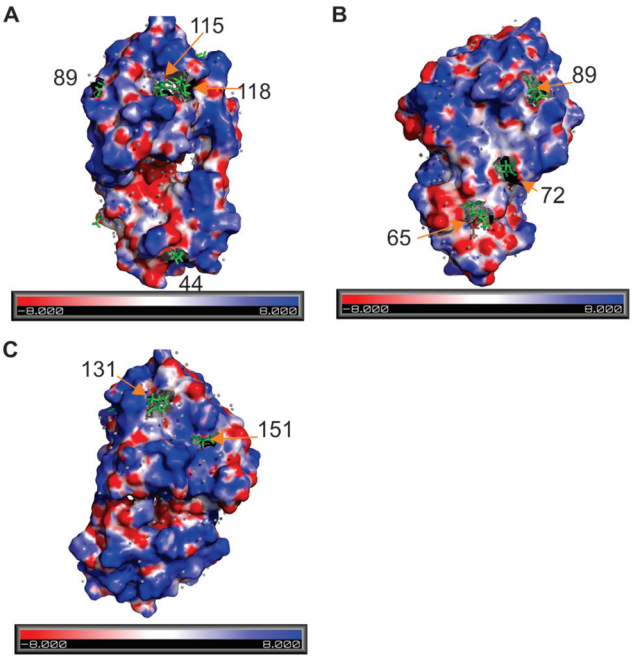

Fig. 7 The surface charge of T4L estimated using PyMOL's APBF function. Three views from different angles were presented to show the location of each studies mutant. Blue: positively charged surface. Red: negatively charged surface.

we propose the docking model of a single protein layer on the OH-SiNPs to be as shown in Fig. 8A, wherein the relative orientation of the protein and the SiNP surface is random. When multiple layers of proteins are formed, since there is no additional broadening detected in the EPR spectra of all studies sites, a random orientation of proteins loosely adsorbed to the first protein layer of the OH-SiNP surface (Fig. 8B) is again proposed.

For the COOH-SiNPs, at pH 7.0, the surface charge is more negative than that of the OH-SiNPs. The charge–charge interaction might be the dominant driving force for protein adsorption (and the associated EPR spectral broadening). For example, we observed strong broadening in the CW EPR spectra of 44R1, 115R1, and 118R1 because these residues are close to positively charged regions with large areas (Fig. 7A). The 72R1, 89R1, and 131R1 are also in close proximity to positively charged regions (Fig. 7B and C) and therefore showed some broadening. The site of 65R1 is surrounded by negatively charged residues (Fig. 7B), and therefore showed the least possibility to make contact with COOH-SiNP surface (and the least broadening). The 151R1 is close to the C-terminus of the protein, wherein the mobility is intrinsically higher. It is likely that when single enzyme layers are formed on the COOH-SiNPs, T4L tends to make contact with the regions close to residues 44 and 115/118 (Fig. 8C, green spheres). It is also possible for a small amount of T4L to interact with COOH-SiNPs *via* the other few residues (Fig. 8C, magenta spheres). When multiple layers of proteins are formed on the

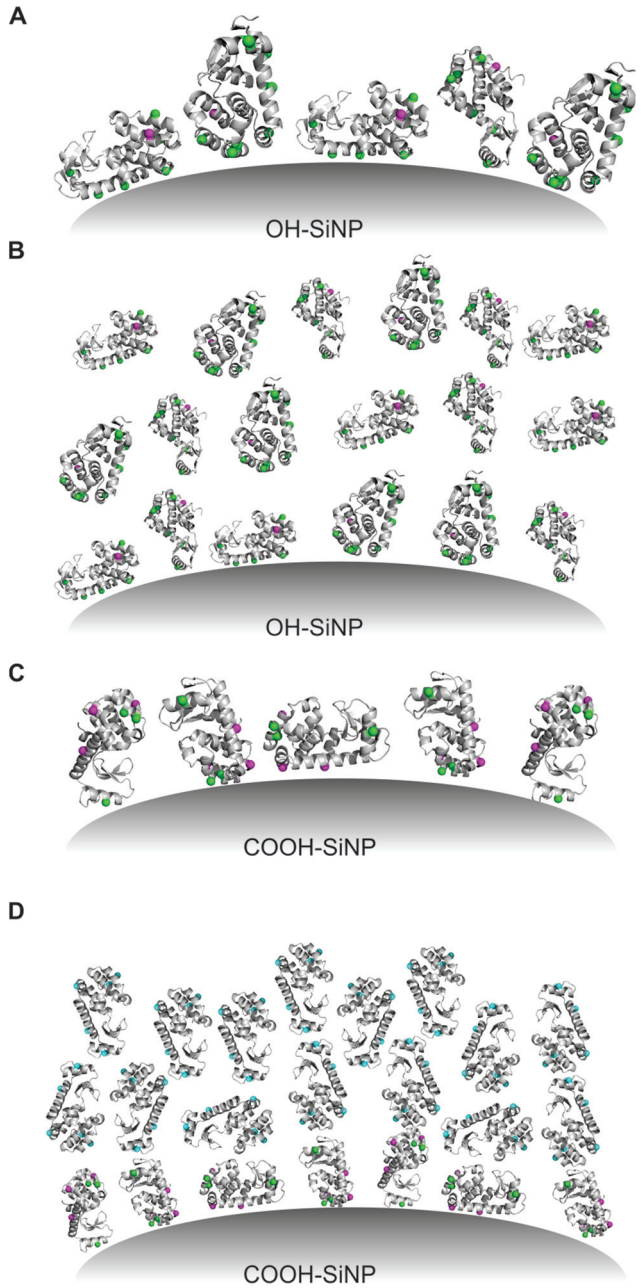

Fig. 8 (A) The proposed adsorption model for the OH-SiNPs when a single layer of T4L is adsorbed. The green dots highlight the preferred contact point, while the magenta ones show the less favored contact point, as judged by CW EPR. (B) When the OH-SiNPs were saturated with T4L, the orientation of each protein is random, and the packing between protein layers is relatively loose. (C) On the COOH-SiNPs, when a single layer of T4L is formed, three sites are favored (green) while another three (magenta) are less favored but still possible to contact the nanoparticle surface. Two sites (65R1 and 151R1) were found to be unlikely to make the contact. The model shows certain preferences in protein orientation relative to the particle surface. (D) When the COOH-SiNPs are saturated with T4L, three sites locating near the N- and the C-terminus were found to face more crowding due to packing (cyan).

COOH-SiNPs, it is more likely for sites 44R1, 65R1, 89R1, 131R1, and 151R1 to face crowding (cyan spheres of Fig. 8D), meaning these regions are more likely to make contact with other proteins.

The multiplex adsorption scheme is possible because of the special surface charge distribution of T4L (Fig. 7). For example, upon adsorption to the SiNP surface with the positively charged N-terminus (Fig. 7C) to form the first adsorption layer, a T4L molecule likely positions its regionally negatively charged C-terminus away from the particle, forming a secondary negatively charged surface. This surface facilitates adsorption of the next layer of enzymes.

Influence of ionic strength

The charge–charge interaction is expected to be influenced by the ionic strength of the medium. To probe such influence, we prepared water medium with different NaCl concentrations (300, 100, and 25 mM; details see Fig. S8 and ESI†). The overall findings are that increasing the ionic strength decreases the adsorption and the ionic strength has a bigger impact on the adsorption of T4L enzyme on the COOH-SiNPs than on the OH-SiNPs. The latter is rationalized to the fact that at pH of 7, the surface of the OH-SiNPs is relatively more neutral than that of the COOH-SiNPs.

Experimental

Protein expression, purification, spin labeling, and characterization

Eight T4L mutants, 44C, 65C, 72C, 89C, 115C, 118C, 131C, and 151C, were created *via* site-directed mutagenesis as described in the literature.[53] These mutants were expressed, purified, and spin labeled using procedures described in our recent work.[54] The spin-labeled mutants were confirmed to have the correct secondary structure and activity *via* CD spectroscopy and an activity assay, respectively, both of which were described in our recent work.[54] A few representative sites were characterized *via* CW EPR to confirm the local conformational dynamics.

Continuous-wave EPR spectroscopy

The typical sample concentration for our CW EPR studies was ~100 μM. Approximately 20 μL of sample was utilized in each measurement. A Varian E-109 spectrometer fitted with a cavity resonator was used for all CW EPR studies.

Preparation of the OH-SiNPs, the NH2-SiNPs, and the COOH-SiNPs

The classical Stöber method was employed to prepare the OH-SiNPs.[55] The particle size of the OH-SiNPs was estimated to be ~30 nm as judged by TEM (see below). The NH2-SiNPs were prepared based on the modification of the OH-SiNPs as described in the ESI.† A severe aggregation was observed for NH2-SiNPs. The COOH-SiNPs were prepared *via* further modi-

fication of the NH2-SiNPs. The final COOH-SiNPs have better dispersity.

Fourier transformation infrared (FTIR)

FTIR spectroscopy spectra of the OH-SiNPs, the NH2-SiNPs, and the COOH-SiNPs were acquired with an FTIR spectrometer (Thermo Scientific Nicolet 8700) on potassium bromide (KBr) disk. The broad absorption peak at 3300–3600 cm^{-1} and the peak at 2980 cm^{-1} indicated the presence of the OH-SiNPs. The absorption peak at 1486 cm^{-1} indicates the existence of $-NH_2$ group on NH2-SiNPs. The absorption peaks at 1557 and 1722 cm^{-1} are consistent with the COOH groups on SiNPs.

Zeta potential measurements

All zeta potential measurements were carried out with a Nano ZS Zetasizer (Malvern Instrument Ltd). Typical sample volume is 5 μL for each of the three SiNPs (5 folds). At pH 7.0, the OH-SiNPs and the COOH-SiNPs were found to have negative surface charges, while the NH2-SiNPs were found to have positive surface charges.

TEM

A drop of the sample was placed on a 300-mesh formvar-carbon coated copper TEM grid (Electron Microscopy Sciences, Hatfield, Pennsylvania, USA) for 30 seconds and wicked off. Phosphotungstic acid 0.1%, pH adjusted to 7–8, was dropped onto the grid, allowed to stand for 2 minutes and then wicked off. After the grids were dry, images were obtained using a JEOL JEM-2100 LaB_6 transmission electron microscope (JEOL USA, Peabody, Massachusetts) running at 200 kV. Phosphotungstic acid is a negative stain that stains the outside of the particles. This gives the particles contrast when subjected to the electron beam in the TEM.

Activity

The activity assay was tested using the kit purchased from Sigma-Aldrich (*Micrococcus lysodeikticus* cells, ATCC no. 4698, M3770) as described earlier in previous reports was used,[54] except that the protein–SiNPs mixtures were used to interact with the *Micrococcus* suspension. To eliminate the possibility of SiNPs affecting OD@450 nm, a series of control experiments were conducted.

DEER EPR

Four-pulse DEER data at 80 K were obtained on an ELEXSYS 580 spectrometer operated at Q-band. Typical final protein concentration is $\lesssim$200 μM, with a typical sample volume of ~20 μL. All samples were flash frozen in water. Distance distributions were obtained from the raw dipolar evolution data using the program "LongDistances" (http://www.chemistry.ucla.edu/directory/hubbell-wayne-l).

Desorption

Desorption experiments were conducted for both saturated OH- and COOH-SiNPs. A representative mutant, $151R_1$, was adsorbed to both SiNPs and washed with 2 × 200 μL HCl buffer (pH = 3, 0.01 M NaCl). Details of each experiment listed above are provided in the ESI.†

AFM imaging

The imaging measurements were performed using a commercial atomic force microscope (NT-MDT NTEGRA AFM). The samples were imaged under ambient conditions in semi-contact mode with a resonant frequency of 190 kHz AFM probes (Budget sensors).

DLS

The DLS data were obtained by using the Zetasizer (NICOMP 380 ZLS particle sizer, Particle Sizing Systems, Inc., USA) at the Department of Coating and Polymeric Materials at NDSU.

Conclusions

A comprehensive study of the structure, dynamics, and activity of a model enzyme upon adsorption to a few surface-modified SiNPs using EPR spectroscopy in combination with several other experimental techniques is reported here. The TEM demonstrated the adsorption of T4L onto two of the prepared SiNPs. The activity assay indicated a significant loss in enzyme activity. To probe the structural basis of such activity loss, the EPR spectroscopy was employed, which overcomes the challenges in probing structural information at the complex and dynamic nano–bio interface. It was found to be possible to estimate the amount of proteins in the hard corona of the SiNPs *via* the CW EPR area analysis. The COOH-SiNPs have a higher loading capacity of T4L enzyme than that of the OH-SiNPs. By comparing the CW EPR spectra of eight studied sites when the mutants were adsorbed to larger sepharose beads and when different protein-to-SiNP ratios were adsorbed to different SiNPs, the residues responsible for making contact with SiNPs and/or facing more crowding under various protein-to-SiNP ratios were identified. Based on this a structural model to depict the docking of T4L onto the SiNPs with different surfaces was proposed. Also the global structural changes caused by adsorption was probed *via* DEER EPR, which served as a second view of the structural basis of the activity loss. Lastly, it was found that the adsorbed enzyme could be desorbed *via* pH adjustment, which showed the potential to use SiNPs for enzyme/protein delivery or storage due to the high capacity. Future work will be directed to tune the properties of SiNPs so that the activity loss can be minimized and SiNPs can be used as enzyme hosts. Our results also highlight the use of EPR in probing structural information on the complex and dynamic inorganic/nano and biological interface.

Acknowledgements

We thank Prof. Wayne Hubbell and Dr Christian Altenbach (UCLA) for generously providing the gene of the pseudo-wild

type T4L, consultation on protein expression, and providing the CW EPR signal acquisition and data analysis software. We also thank Prof. Wayne Hubbell for accessing the DEER facility at his laboratory. This work is supported by NSF ND EPSCoR start-up funds, NDSU Department of Chemistry and Biochemistry Center for Protease Research of NIH, and young faculty start-up funds of NDSU College of Science and Mathematics. The TEM work is supported by the National Science Foundation under Grant No. 0821655. Any opinions, findings, and conclusions or recommendations expressed in this material are those of the author(s) and do not necessarily reflect the views of the National Science Foundation.

Notes and references

1 M. I. Kim, H. O. Ham, S.-D. Oh, H. G. Park, H. N. Chang and S.-H. Choi, *J. Mol. Catal. B: Enzym.*, 2006, **39**, 62–68.
2 F. Zhao, T. Hou, J. Wang, Y. Jiang, S. Huang, Q. Wang, M. Xian and X. Mu, *Bioprocess Biosyst. Eng.*, 2017, **40**, 1–7.
3 S. Zhang, H. Lu and Y. Lu, *Environ. Sci. Technol.*, 2013, **47**, 13882–13888.
4 L. Tang and J. Cheng, *Nano Today*, 2013, **8**, 290–312.
5 M. Ravera, E. Gabano, I. Zanellato, E. Perin, A. Arrais and D. Osella, *Dalton Trans.*, 2016, **45**, 17233–17240.
6 Z. Xu, S. Liu, Y. Kang and M. Wang, *Nanoscale*, 2015, **7**, 5859–5868.
7 D. Tarn, C. E. Ashley, M. Xue, E. C. Carnes, J. I. Zink and C. J. Brinker, *Acc. Chem. Res.*, 2012, **46**, 792–801.
8 C. J. López, M. R. Fleissner, Z. Guo, A. K. Kusnetzow and W. L. Hubbell, *Protein Sci.*, 2009, **18**, 1637–1652.
9 C. Altenbach, C. J. López, K. Hideg, W. L. Hubbell, Z. Q. Peter and W. Kurt, in *Methods in Enzymology*, Academic Press, 2015, vol. 564, pp. 59–100.
10 C. J. López, M. R. Fleissner, E. K. Brooks and W. L. Hubbell, *Biochemistry*, 2014, **53**, 7067–7075.
11 Z. Yang, Y. Liu, P. Borbat, J. L. Zweier, J. H. Freed and W. L. Hubbell, *J. Am. Chem. Soc.*, 2012, **134**, 9950–9952.
12 Y. Kim, S. M. Ko and J.-M. P. Nam, *Chem. – Asian J.*, 2016, **11**, 1869–1877.
13 M. Mahmoudi, I. Lynch, M. R. Ejtehadi, M. P. Monopoli, F. B. Bombelli and S. Laurent, *Chem. Rev.*, 2011, **111**, 5610–5637.
14 I. Lynch and K. A. Dawson, *Nano Today*, 2008, **3**, 40–47.
15 H. Pan, M. Qin, W. Meng, Y. Cao and W. Wang, *Langmuir*, 2012, **28**, 12779–12787.
16 S. R. Saptarshi, A. Duschl and A. L. Lopata, *J. Nanobiotechnol.*, 2013, **11**, 1–12.
17 C. Gunawan, M. Lim, C. P. Marquis and R. Amal, *J. Mater. Chem. B*, 2014, **2**, 2060–2083.
18 J. Lazarovits, Y. Y. Chen, E. A. Sykes and W. C. W. Chan, *Chem. Commun.*, 2015, **51**, 2756–2767.
19 C. Ge, J. Tian, Y. Zhao, C. Chen, R. Zhou and Z. Chai, *Arch. Toxicol.*, 2015, **89**, 519–539.
20 L. Treuel, S. Brandholt, P. Maffre, S. Wiegele, L. Shang and G. U. Nienhaus, *ACS Nano*, 2014, **8**, 503–513.
21 N. P. Mortensen, G. B. Hurst, W. Wang, C. M. Foster, P. D. Nallathamby and S. T. Retterer, *Nanoscale*, 2013, **5**, 6372–6380.
22 R. Huang, R. P. Carney, F. Stellacci and B. L. T. Lau, *Nanoscale*, 2013, **5**, 6928–6935.
23 E. Casals, T. Pfaller, A. Duschl, G. J. Oostingh and V. Puntes, *ACS Nano*, 2010, **4**, 3623–3632.
24 H. S. McHaourab, P. R. Steed and K. Kazmier, *Structure*, 2011, **19**, 1549–1561.
25 D. S. Cafiso, *Acc. Chem. Res.*, 2014, **47**, 3102–3109.
26 A. L. Turner, O. Braide, F. D. Mills, G. E. Fanucci and J. R. Long, *Biochim. Biophys. Acta, Biomembr.*, 2014, **1838**, 3212–3219.
27 G. E. Fanucci and D. S. Cafiso, *Curr. Opin. Struct. Biol.*, 2006, **16**, 644–653.
28 H. A. DeBerg, P. S. Brzovic, G. E. Flynn, W. N. Zagotta and S. Stoll, *J. Biol. Chem.*, 2016, **291**, 371–381.
29 Z. Yang, M. R. Kurpiewski, M. Ji, J. E. Townsend, P. Mehta, L. Jen-Jacobson and S. Saxena, *Proc. Natl. Acad. Sci. U. S. A.*, 2012, **109**, E993–E1000.
30 X. Zhang, S. W. Lee, L. Zhao, T. Xia and P. Z. Qin, *RNA*, 2010, **16**, 2474–2483.
31 C. Vazquez Reyes, N. S. Tangprasertchai, S. D. Yogesha, R. H. Nguyen, X. Zhang, R. Rajan and P. Z. Qin, *Cell Biochem. Biophys.*, 2016, 1–8.
32 S. Ling, W. Wang, L. Yu, J. Peng, X. Cai, Y. Xiong, Z. Hayati, L. Zhang, Z. Zhang, L. Song and C. Tian, *Sci. Rep.*, 2016, **6**, 20025.
33 M. Ji, S. Ruthstein and S. Saxena, *Acc. Chem. Res.*, 2014, **47**, 688–695.
34 K. Kawasaki, J.-J. Yin, W. K. Subczynski, J. S. Hyde and A. Kusumi, *Biophys. J.*, 2001, **80**, 738–748.
35 S. Pornsuwan, G. Bird, C. E. Schafmeister and S. Saxena, *J. Am. Chem. Soc.*, 2006, **128**, 3876–3877.
36 A. Godt, M. Schulte, H. Zimmermann and G. Jeschke, *Angew. Chem., Int. Ed.*, 2006, **45**, 7560–7564.
37 A. Doll, M. Qi, N. Wili, S. Pribitzer, A. Godt and G. Jeschke, *J. Magn. Reson.*, 2015, **259**, 153–162.
38 W. L. Hubbell, C. J. López, C. Altenbach and Z. Yang, *Curr. Opin. Struct. Biol.*, 2013, **23**, 725–733.
39 P. Borbat and J. Freed, in *Structural Information from Spin-Labels and Intrinsic Paramagnetic Centers in the Biosciences. Structure and Bonding*, ed. J. Harmer, C. Timmel, Springer, Heidelberg, Germany, New York, USA, 2014, vol. 152, pp. 1–82.
40 G. Jeschke, *Annu. Rev. Phys. Chem.*, 2012, **63**, 419–446.
41 Z. Yang, M. Bridges, M. T. Lerch, C. Altenbach, W. L. Hubbell, Z. Q. Peter and W. Kurt, in *Methods in Enzymology*, Academic Press, 2015, vol. 564, pp. 3–27.
42 M. G. Grütter and B. W. Matthews, *J. Mol. Biol.*, 1982, **154**, 525–535.
43 C. K. Bower, Q. Xu and J. McGuire, *Biotechnol. Bioeng.*, 1998, **58**, 658–662.
44 H. S. Mchaourab, M. A. Lietzow, K. Hideg and W. L. Hubbell, *Biochemistry*, 1996, **35**, 7692–7704.

45 J. McCoy and W. L. Hubbell, *Proc. Natl. Acad. Sci. U. S. A.*, 2011, **108**, 1331–1336.
46 W. L. Hubbell and C. Altenbach, *Curr. Opin. Struct. Biol.*, 1994, **4**, 566–573.
47 A. P. Todd, J. Cong, F. Levinthal, C. Levinthal and W. L. Hubbell, *Proteins: Struct., Funct., Bioinf.*, 1989, **6**, 294–305.
48 Z. Guo, D. Cascio, K. Hideg and W. L. Hubbell, *Protein Sci.*, 2008, **17**, 228–239.
49 R. Langen, K. J. Oh, D. Cascio and W. L. Hubbell, *Biochemistry*, 2000, **39**, 8396–8405.
50 R. G. Larsen and D. J. Singel, *J. Chem. Phys.*, 1993, **98**, 5134–5146.
51 P. P. Borbat, J. H. Freed, M. I. Simon, B. R. Crane and C. Alexandrine, in *Methods in Enzymology*, Academic Press, 2007, vol. 423, pp. 52–116.
52 C. J. López, Z. Yang, C. Altenbach and W. L. Hubbell, *Proc. Natl. Acad. Sci. U. S. A.*, 2013, **110**, E4306–E4315.
53 Z. Yang, G. Jiménez-Osés, C. J. López, M. D. Bridges, K. N. Houk and W. L. Hubbell, *J. Am. Chem. Soc.*, 2014, **136**, 15356–15365.
54 S. Neupane, Y. Pan, S. Takalkar, K. Bentz, J. Farmakes, Y. Xu, B. Chen, G. Liu, S. Qian and Z. Yang, *J. Phys. Chem. C*, 2017, **121**, 1377–1386.
55 W. Stöber, A. Fink and E. Bohn, *J. Colloid Interface Sci.*, 1968, **26**, 62–69.